NJC

New Journal of Chemistry

A journal for new directions in chemistry

Accepted Manuscript

This article can be cited before page numbers have been issued, to do this please use: S. N. M. Sharif, N. Hashim, M. I. Illyas, S. Abu Bakar, M. I. Saidin, M. S. Ahmad, M. Mamat, M. Z. Hussein and R. Zainul, *New J. Chem.*, 2020, DOI: 10.1039/D0NJ01315C.

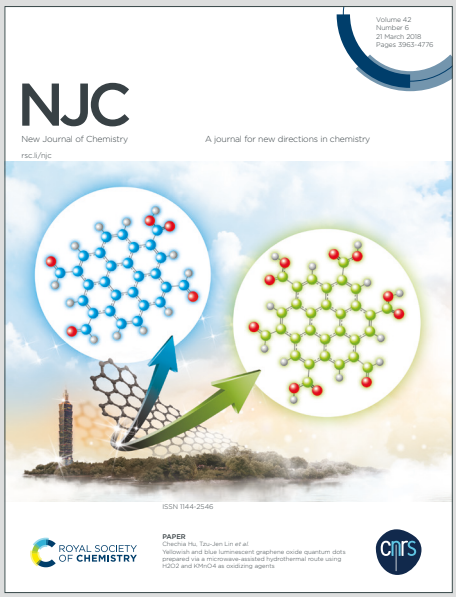

This is an Accepted Manuscript, which has been through the Royal Society of Chemistry peer review process and has been accepted for publication.

Accepted Manuscripts are published online shortly after acceptance, before technical editing, formatting and proof reading. Using this free service, authors can make their results available to the community, in citable form, before we publish the edited article. We will replace this Accepted Manuscript with the edited and formatted Advance Article as soon as it is available.

You can find more information about Accepted Manuscripts in the Information for Authors.

Please note that technical editing may introduce minor changes to the text and/or graphics, which may alter content. The journal's standard Terms & Conditions and the Ethical guidelines still apply. In no event shall the Royal Society of Chemistry be held responsible for any errors or omissions in this Accepted Manuscript or any consequences arising from the use of any information it contains.

View Article Online
DOI: 10.1039/D0NJ01315C

ARTICLE

The Impact of Hygroscopic Chitosan Coating on the Controlled Release Behaviour of Zinc hydroxide nitrate–Sodium Dodecylsulphate–Imidacloprid Nanocomposite

Received 00th January 20xx,
Accepted 00th January 20xx

DOI: 10.1039/x0xx00000x

Sharifah Norain Mohd Sharif[a], Norhayati Hashim*[a,b], Illyas Md Isa [a,b], Suriani Abu Bakar[c], Mohamad Idris Saidin[a], Mohamad Syahrizal Ahmad[a], Mazidah Mamat[d], Mohd Zobir Hussein[e] and Rahadian Zainul[f]

Imidacloprid (IC) is a neutral charge insecticide that is commonly used in paddy cultivation areas to kill invasive insects. However, the uncontrollable usage of IC may cause serious problems toward the non–target organisms and environment. This work focussed on the potential of using chitosan to develop an efficient insecticide that could minimise the environmental risk by controlling the release of the IC into the environment. The powder X-ray diffraction (PXRD) and Fourier transform infrared (FTIR) analysis of the chitosan coated zinc hydroxide nitrate–sodium dodecylsulphate–imidacloprid (ZHN–**SDS**–IC–Chi) nanocomposite confirmed that the chitosan coating process did not interfere with the type of ions that were intercalated in the interlayer gallery of the nanocomposite. The release study performed in aqueous solutions of Na_3PO_4, Na_2SO_4 and NaCl revealed that the slowest release was observed when using NaCl as the release media. The release of IC was governed by the pseudo second order kinetic model, which described the release mechanism of the IC as being via dissolution and ion exchange. Even though the overall findings showed that the physicochemical properties of the ZHN–**SDS**–IC and ZHN–**SDS**–IC–Chi were not too different, the presence of chitosan was found to be beneficial in prolonging the release process. The synthesised ZHN–**SDS**–IC–Chi nanocomposite will hopefully be used as a safer insecticide in paddy cultivation and will fulfil both economic and ecological demands.

1. Introduction

It has long been recognised that controlled release technologies possess great potential in various sectors, including agricultural, pharmaceutical and food industries.[1–7] In the agricultural sector, the implementation of a controlled release formulation (**CRF**) into pesticides helps to prolong the release of the pesticide.[8,9] The excessive use of pesticides is not only costly, but also risky to the environment.[10,11] Therefore, the **CRF** in pesticide implies that the formulations involved are so created as to deliver the proper dosage for effective long or short term pest control. Pesticide integrated with **CRF** is an endeavour to develop the ideal delivery system of the pesticide and allow a sufficient release of the pesticide that will effectively exterminate pests while preserving the environment.[12] Releasing the pesticide in slow and sustainable manner will assist in preventing environmental pollutions by minimising the distribution of excess pesticides residues to the environment (via evaporation, degradation or leaching by rain into the waterway), commonly occurred due to the simultaneous releases of high pesticides concentration.[13]

Zinc hydroxide nitrate (**ZHN**), with the general formula of $Zn_5(OH)_8(NO_3)_2{\cdot}2H_2O$, is amongst attractive layered metal hydroxides that were commonly used as host materials in **CRF**. The positively charged **ZHN** provided an interlayer gallery of a flexible height that can contain a wide range of functional guest anions for **CRF** purpose, including cinnamate, 4-(2,4-dichlorophenoxy)butyrate, 2-(3-chlorophenoxy) propionate and 4-dichlorophenoxy acetate.[14–17] The anions accommodate the interlayer gallery and counterbalance the excessive positive charge generated by the **ZHN** and stabilise the overall charge. The intercalation of anions into the interlayer gallery of the **ZHN**, creates a host–guest nanocomposite that is favourable to **CRF**. Owing to its versatility, **ZHN** can also be intercalated with a neutral charge ion with the assistance of a surfactant.[8] The interaction between the host and guest ions significantly affect the **CRF** behaviour of the nanocomposite in terms of diffusion, release rate and other physicochemical properties.[12] A previous study showed that the intercalation of the guest ions was successfully performed via direct reaction, ion exchange and reconstruction methods.[4,17–20] Although the potential of **ZHN** as an ideal host for **CRF** has been acknowledged, the delivery efficiency of the nanocomposite can be further improved by introducing a biopolymer

[a.] *Department of Chemistry, Faculty of Science and Mathematics, Universiti Pendidikan Sultan Idris, 35900 Tanjong Malim, Perak, Malaysia.*
[b.] *Nanotechnology Research Centre, Faculty of Science and Mathematics, Universiti Pendidikan Sultan Idris, 35900 Tanjong Malim, Perak, Malaysia.*
[c.] *Department of Physics, Faculty of Science and Mathematics, Universiti Pendidikan Sultan Idris, 35900 Tanjong Malim, Perak, Malaysia.*
[d.] *School of Fundamental Science, Universiti Malaysia Terengganu, 21030 Kuala Terengganu, Terengganu, Malaysia.*
[e.] *Materials Synthesis and Characterization Laboratory, Institute of Advanced Technology, Universiti Putra Malaysia, 43400 Serdang, Selangor, Malaysia.*
[f.] *Department of Chemistry, Faculty of Mathematics and Natural Science, Universitas Negeri Padang, West Sumatera 25171, Indonesia.*
**Corresponding author, E-mail: norhayati.hashim@fsmt.upsi.edu.my; Phone: +6015 4879 7314; Fax: +6015 4879 7296*

View Article Online DOI: 10.1039/D0NJ01315C

material as a coating for the nanocomposite. Chitosan, a well–studied polysaccharide derived by partial N–deacetylation of chitin, is a potential coating for the pesticides with **CRF** due to its biodegradability, mucoadhesive properties, non–toxic nature, ability of form a film and gel.[21,22] Free amino groups that were present in its structure make it insoluble in neutral or basic media. Hence, the use of an acid is needed to complete the solubilization so that the amino group can be protonated and the polymer can swell.[23] Chitosan was previously reported to be used in the controlled release of curcumin, aspirin, solid lipid nanoparticle and NPK fertilisers.[21,22,24,25] The incorporation of chitosan was also reported to enhance the thermal stability of the particular compound.[26] The chemical structure of chitosan is shown in Fig. 1.

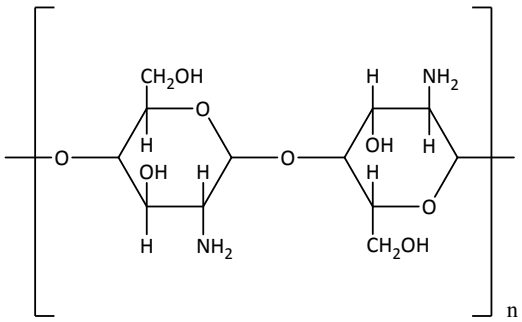

Fig. 1 The chemical structure of chitosan.

Imidacloprid (**IC**) is a neonicotinoid, neutral charge insecticide that widely used in paddy cultivation area to kill invasive insects such as brown planthopper, white–backed planhopper and small brown planthopper.[27] The chemical structure of **IC** is shown in Fig. 2. Similar to other neonicotinoid insecticide, **IC** penetrate into the central nervous system of these insect, and disturbing their nicotinic acetylcholine receptors.[28–30] Due to the neutral charge nature of IC, this insecticide may not be directly intercalated into the interlayer gallery of **ZHN**. However, our recently published paper has reported on the possibility of intercalating **IC** into the ZHN with the assistance of sodium dodecylsulphate (**SDS**), by creating hydrophobic region in the interlayer gallery, thus assisting the intercalation process.[31]

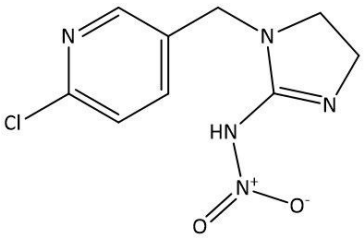

Fig. 2 The chemical structure of imidacloprid.

In this present paper, an attempt to enhance the controlled release properties of the zinc hydroxide nitrate–sodium dodecylsulphate–imidacloprid (**ZHN–SDS–IC**) nanocomposite was carried out by coating the **ZHN–SDS–IC** nanocomposite with chitosan (the coated nanocomposite will be denoted as **ZHN–SDS–IC–Chi**). The characterisation studies were subsequently performed on the **ZHN–SDS–IC–Chi** to examine the effect of the chitosan coating on the physicochemical properties of the nanocomposite. The controlled release study of **ZHN–SDS–IC–Chi** was investigated under similar experimental conditions as for **ZHN–SDS–IC**, and their release behaviour was then observed and compared. To the best of the authors' knowledge, no study has yet been reported on the potential of **ZHN–SDS–IC–Chi** as a **CRF** for a pesticide. A schematic representation of the present study was shown in Fig. 3.

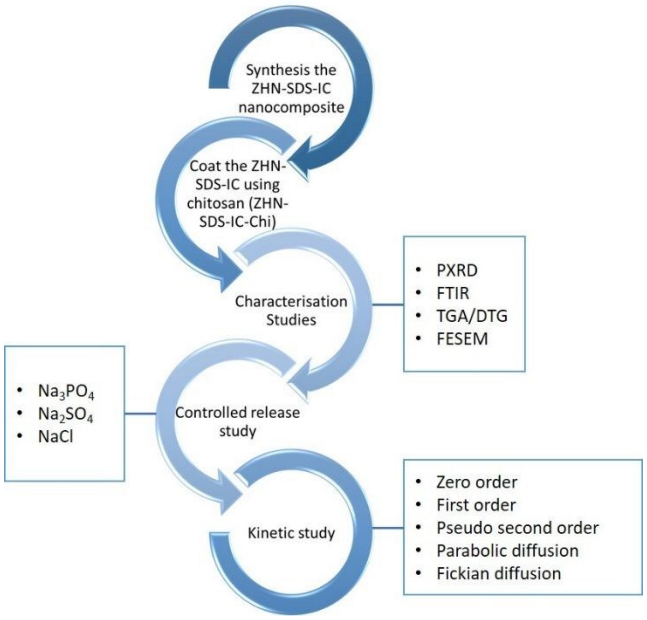

Fig. 3 The schematic representation of the study

2. Experimental

2.1 Materials

The $Zn(NO_3)_2{\cdot}6H_2O$ (purity 98%) and **SDS** were purchased from Systerm (Malaysia). The **IC** that was intercalated in the interlayer gallery of **ZHN–SDS** was bought from Essense (China) with a purity of 98%. The glacial acetic acid and chitosan were supplied by Systerm (Malaysia) and Sigma Aldrich (USA), respectively. The release media were prepared using sodium phosphate (Na_3PO_4), sodium sulphate (Na_2SO_4) and sodium chloride (NaCl). The Na_3PO_4 (purity 99.5 %) was supplied by Merck (Germany), whereas both the Na_2SO_4 (purity 95.2%) and NaCl (purity 99.0%) were purchased from Systerm (Malaysia). All reagents in the study were used as–received and without further purification. The deionised water was used as a solvent to prepare all solutions.

2.2 Synthesis of ZHN–SDS–IC, ZHN–SDS–Chi and ZHN–SDS–IC–Chi nanocomposite

The **ZHN–SDS** was prepared by co–precipitation using $Zn(NO_3)_2{\cdot}6H_2O$ and **SDS** as the precursors. The **ZHN–SDS–IC** nanocomposite was

then synthesised by mixing the **ZHN–SDS** into the **IC** solution and stirring constantly for 24 h. The procedure to synthesis the **ZHN–SDS** and **ZHN–SDS–IC** was described in a paper previously published by the authors.[31]

The synthesis of the chitosan coated **ZHN–SDS–IC** nanocomposite (denoted as **ZHN–SDS–IC–Chi**) was started by preparing the chitosan solution for the coating process. A quantity of 0.1 g chitosan was weighed and dissolved in 1% glacial acetic acid. As gelation of the chitosan began, it was heated for 30 minutes under magnetic stirring to dissolve the chitosan. Then, 50 mL of deionised water was then added into the mixture and it was continuously stirred at room temperature for 24 h to completely dissolve the chitosan. Next, 0.1 g of the **ZHN–SDS–IC** nanocomposite was added into the mixture and it was continuously stirred for 18 h. The **ZHN–SDS–IC–Chi** nanocomposite was collected by centrifugation (4000 rpm for 5 min) and dried in an oven (at 60 °C for 24 h). The product was ground and kept in a sample bottle. The **ZHN–SDS** was also coated using a similar procedure, and it was denoted as **ZHN–SDS–Chi**.

2.3 Characterisation

Powder X–ray diffraction (**PXRD**) was carried out on a PANalytical X–pert Pro MPD diffractometer using Co K–alpha radiation (λ = 1.54056 Å). The **PXRD** measurements were conducted at room temperature, with the Bragg angle ranging from 2 to 60°, a scanning speed of 2˚/min, step size of 0.0330° and scan step time of 9.4434 s. The **PXRD** instrument used an operating voltage and current of 40 kV and 30 mA, respectively. The Fourier transform infrared (**FTIR**) spectra were performed on a Nicolet **FTIR** spectrometer (400–4000 cm^{-1}). The nominal resolution of the **FTIR** was set to 4 cm^{-1} and the samples were compressed in a KBr disk with a mass ratio (sample/KBr) of 1:100. Thermal behaviour of the samples was studied by thermogravimetric analysis and differential thermal analysis (**TGA/DTG**). The measurements were performed on Perkin Elmer Pyris 1 TGA thermo balance in nitrogen gas at a heating rate of 10 °C/min and in the range 35−1000 °C. The surface morphology of the samples was probed using field emission scanning electron microscope (FESEM, Hitachi SU 8020 UHR).

2.4 Controlled Release Formulation Study of ZHN–SDS–IC–Chi nanocomposite

The amount of **IC** that was released from the interlayer gallery of the **ZHN–SDS–IC–Chi** nanocomposite was measured by a Lambda 25 Perkin Elmer ultraviolet–visible (UV/Vis) spectrometer (λ_{max} = 269.5). The experimental conditions for the UV/Vis spectrometer included a time interval of 60 s, slit width of 1.0 nm, lamp change of 326.0 nm, ordinate max of 1.0 and ordinate min of 0.0. The release media were prepared using an aqueous solution of Na_3PO_4, Na_2SO_4 and NaCl, each prepared in three concentrations: 0.1 M, 0.3 M and 0.5 M. In each measurement, 0.6 mg of the **ZHN–SDS–IC–Chi** nanocomposite was released in 3.5 mL of release media and left for several days until the absorbance reading become constant. The accumulated percentage release of the **IC** was calculated using a standard calibration curve that was obtained from a series of standard solutions of **IC**. In order to understand the mechanism of release, the release data were then fitted into five kinetic models: zero order, first order, pseudo second order, parabolic diffusion and Fickian diffusion models. This was done so that the release mechanism could be examined in detail.

3. Results and discussion

3.1 PXRD Analysis

The **PXRD** analysis was beneficial in determining the crystallinity of the nanocomposite before and after it was coated with chitosan.[23] The **PXRD** patterns of the chitosan, **ZHN–SDS**, **ZHN–SDS–IC**, **ZHN–SDS–Chi** and **ZHN–SDS–IC–Chi** are presented in Fig. 4. Based on the **PXRD** patterns, an obvious and broad peak, with basal spacing of 4.5 Å, was spotted in the **PXRD** pattern of the chitosan, indicating the typical amorphous structure. The amorphous peak of the chitosan is in good agreement with previous results in the literature.

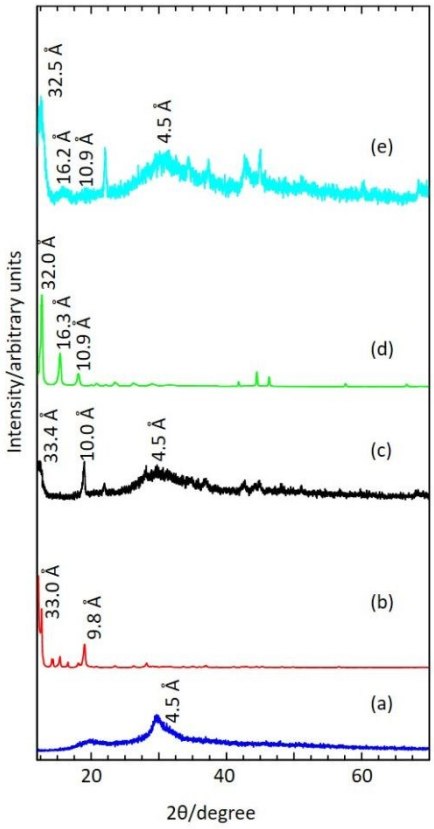

Fig. 4 PXRD patterns of (a) chitosan, (b) ZHN–SDS, (c) ZHN–SDS–Chi, (d) ZHN–SDS–IC[31] and (e) ZHN–SDS–IC–Chi.

The major characteristic peaks for the **ZHN–SDS**, with a basal spacing of 32.0 Å and 9.8 Å, were symmetrical, intense and sharp, thus signifying their highly crystalline nature. These peaks were also detected in the **PXRD** pattern for the **ZHN–SDS** (basal spacing of 33.4 Å and 10.0 Å) after it is coated with chitosan, although the intensity of the peaks was greatly reduced due to the presence of the amorphous chitosan. The presence of the chitosan in the **ZHN–SDS–Chi** was also confirmed and was based on the appearance of the characteristic peak of chitosan (basal spacing of 4.5 Å) in the **PXRD** pattern. The chitosan characteristic peak was also observed in the **PXRD** pattern for the **ZHN–SDS–IC–Chi**.

View Article Online
DOI: 10.1039/D0NJ01315C

The **ZHN–SDS–IC** showed an intense intercalation peak at a lower angle of 2θ, with basal spacing of 32.0 Å, 16.3 Å and 10.9 Å, owing to the presence of the well crystallized **ZHN–SDS–IC**. Similar peaks can also be seen in the **PXRD** pattern for the **ZHN–SDS–IC–Chi** (basal spacing of 32.5 Å, 16.2 Å and 10.9 Å). The intercalation peaks of the **ZHN–SDS–IC–Chi** overlapped with the noise that originated from the chitosan, which made it visibly less obvious compared to the peaks for the **ZHN–SDS–IC** nanocomposite. In fact, the amorphous chitosan coating process diminished the peaks and caused them to appear as flattened humps instead of as sharp peaks. The conversion from a well crystallized structure into an amorphous one provided additional evidence for the success of the chitosan coating of the **ZHN–SDS–IC**. The changes in the **PXRD** pattern after the chitosan coating are in good agreement with the previous study.[32,33]

The **PXRD** analysis also revealed that the chitosan coating process on both **ZHN–SDS** and the **ZHN–SDS–IC** did not cause any major changes in the interlayer distance. Although not all basal spacing values of the peaks in the **PXRD** pattern of the **ZHN–SDS** and the **ZHN–SDS–IC** remained exactly the same, the changes were very insignificant. Hence, this indicated that the chitosan coating process did not interfere with the ions intercalated in the interlayer gallery for both **ZHN–SDS** and **ZHN–SDS–IC**.

The **ZHN–SDS–IC** that were coated in this study were prepared using a similar concentration of IC (0.01 M), as this concentration was found to be the most optimum concentration to be intercalated into **ZHN–SDS** system.[31] Both **ZHN–SDS** and the **ZHN–SDS–IC** synthesised were coated with chitosan, using chitosan to nanocomposite mass ratio of 1:1. This composition was selected based on the good result obtained from the **PXRD** analysis as compare to the other ratio. Therefore, the composition was fixed throughout the study.

3.2. Spatial arrangement of chitosan coated ZHN–SDS–IC nanocomposite

As mentioned in a previous paper by the authors, the height of the interlayer gallery of **ZHN–SDS–IC** was found to be 22.0 Å, whereas the dimension of **IC** and **SDS** were calculated to be 12.5 x 9.2 x 7.2 Å and 19.9 x 6.1 x 5.2 Å, respectively (as predicted by Chem 3D Ultra 8.0 software).[31] Based on this information, the **IC** and **SDS** were believed to be oriented in the interlayer gallery of **ZHN** in a vertical monolayer arrangement.

In this present paper, it was found that after the **ZHN–SDS–IC** were coated with chitosan, the height of the interlayer gallery of the **ZHN–SDS–IC** increased slightly. The basal spacing of the **ZHN–SDS–IC–Chi** was determined to be 32.5 Å (provided by the **PXRD** analysis), the thickness of the **ZHN** was 4.8 Å and the thickness of the Zn tetrahedron was 2.6 Å. Therefore, the height of the interlayer gallery of the **ZHN–SDS–IC–Chi** was 22.5 Å, which is considerably greater for the **ZHN–SDS–IC**. The slight increment in the height of the interlayer gallery after the **ZHN–SDS–IC** was coated with chitosan was due to the **ZHN–SDS–IC–Chi** enabling the vertical monolayer arrangement. The proposed spatial arrangement of the **ZHN–SDS–IC** and the **ZHN–SDS–IC–Chi** nanocomposites are shown in Fig. 5.

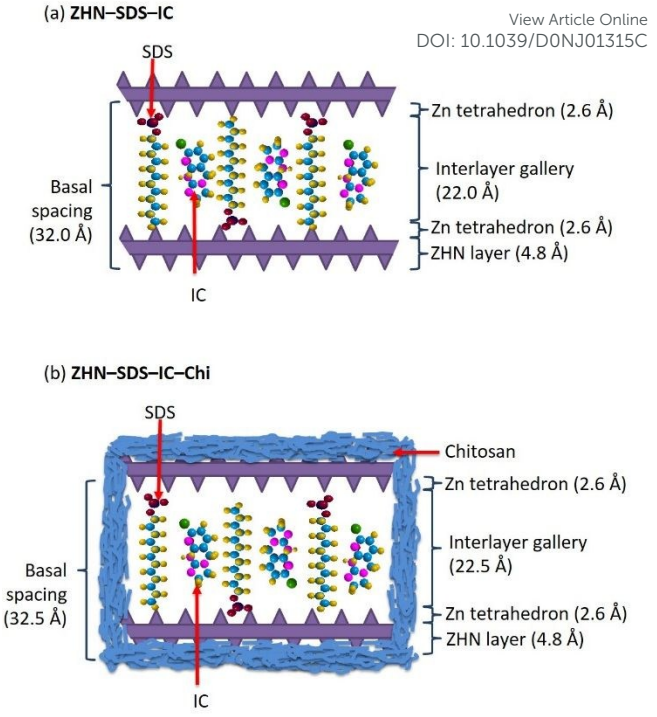

Fig. 5 Spatial orientation of IC and SDS in the interlayer gallery of (a) ZHN–SDS–IC [31] and (b) ZHN–SDS–IC–Chi.

3.3. FTIR analysis

In order to further investigate the impact of the chitosan coating on both **ZHN–SDS** and **ZHN–SDS–IC**, **FTIR** analysis was applied. The results obtained from the **FTIR** analysis is shown in Fig. 6 and also summarised into Table 1. In general, several typical characteristic peaks for the chitosan were observed in the **FTIR** spectra of chitosan at 1665 cm^{-1} (amide I), 1556 cm^{-1} (N–H bending) and 1052 cm^{-1} (C–N stretching from amide).[21–23,34] The broad peak that appeared from the stretching of the hydroxyl group can be observed in the **FTIR** spectra for the **ZHN–SDS**, chitosan, **ZHN–SDS–Chi**, **ZHN–SDS–IC** and **ZHN–SDS–IC–Chi** at 3458 cm^{-1}, 3497 cm^{-1}, 3322 cm^{-1}, 3492 cm^{-1} and 3335 cm^{-1}, respectively.

After the **ZHN–SDS** was coated with chitosan, several peaks that were attributed to **SDS** and chitosan can be seen in the **FTIR** spectra of the **ZHN–SDS–Chi**. The peaks that indicate the presence of **SDS** were observed at 1218 cm^{-1} and 809 cm^{-1} due to the asymmetric stretching of S=O and stretching of S–O, respectively.[35] These peaks were originally found in the **FTIR** spectra of the **ZHN–SDS** at 1217 cm^{-1} and 827 cm^{-1}. The peak that indicated the presence of chitosan in the **ZHN–SDS–Chi** can be seen at 1645 cm^{-1} and 1057 cm^{-1} due to the amide I and C–N stretching, respectively.[21–23,34]

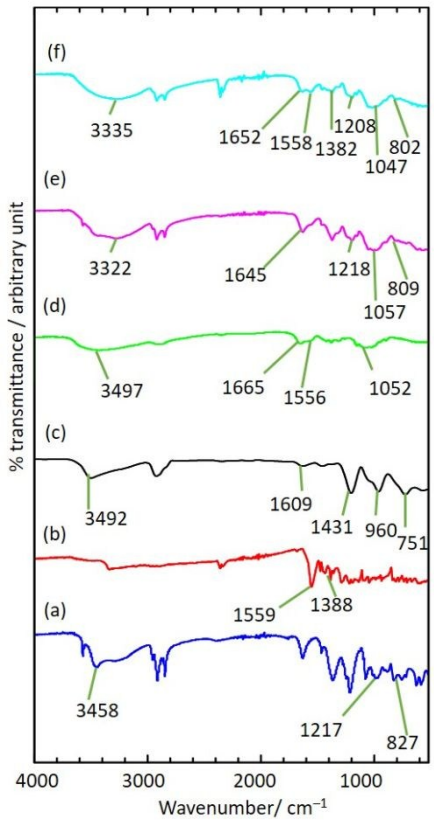

Fig. 6. FTIR spectra for (a) ZHN–SDS[31], (b) IC[31], (c) ZHN–SDS–IC[31], (d) chitosan, (e) ZHN–SDS–Chi and (f) ZHN–SDS–IC–Chi.

Table 1. FTIR Spectra of ZHN–SDS, IC, ZHN–SDS–IC, Chitosan, ZHN–SDS–Chi and ZHN–SDS–IC–Chi

Attribution	ZHN–SDS	IC	ZHN–SDS – IC	Chitosan	ZHN–SDS–Chi	ZHN–SDS–IC–Chi
ν(O–H) in H_2O	3458	–	3492	3497	3322	3335
ν_s(C=C) in amide I	–	–	–	1665	1645	1652
ν_s(C–N) in amide	–	–	–	1556	–	–
ν_s(C–O–C)	–	–	–	1052	1057	1047
ν_{as}(S=O) in SDS	1217	–	960	–	1218	1208
ν_s(S–O) in SDS	827	–	751	–	809	802
Pyridine in IC	–	1559	1609	–	–	1558
ν_s(N–O) in IC	–	1388	1431	–	–	1382
Ref.	31	31	31	Present paper	Present paper	Present paper

In case of the **ZHN–SDS–IC**, the **FTIR** spectra for the **ZHN–SDS–IC–Chi** itself showed some feature of **IC**, **SDS** and chitosan after it was coated. The characteristic peak for the **IC** that was attributed to the pyridine (originally found in the **FTIR** spectra of **IC** and **ZHN–SDS–IC** at 1559 cm^{-1} and 1609 cm^{-1}, respectively) was also observed in the **FTIR** spectra for **ZHN–SDS–IC–Chi** at 1558 cm^{-1}.[35] The peak that signifies the N–O bond in the nitro group of **IC** can be observed in the **FTIR** spectra for the **ZHN–SDS–IC–Chi** at 1382 cm^{-1} and also in both **FTIR** spectra for the **IC** and **ZHN– SDS–IC** at 1388 cm^{-1} and 1431 cm^{-1}, respectively. The appearance of pyridine and N–O peaks therefore prove that the **IC** were loaded in both **ZHN–SDS–IC** and **ZHN–SDS–IC–Chi**. The characteristic peaks for **SDS** can be observed in the **FTIR** spectra for the **ZHN–SDS–IC–Chi** at 1208 cm^{-1} (asymmetric stretching of S=O) and 802 cm^{-1} (stretching of S–O). The characteristic peaks for chitosan were observed at 1652 cm^{-1} (amide I) and 1047 cm^{-1} (C–N stretching from amide).[21–23,34,36,37] Before the **ZHN–SDS–IC** underwent the chitosan coating process, the peak that is assigned to the asymmetric stretching of S=O and S–O were previously observed in the **FTIR** spectra of **ZHN–SDS–IC** at 960 cm^{-1} and 751 cm^{-1}, respectively.

All the aforementioned characteristic peaks that appeared in the **FTIR** spectra show that the chitosan coating did not affect the **SDS** and **IC** that were intercalated in the interlayer gallery of the **ZHN–SDS**. Hence, it can be concluded that the result obtained from the **FTIR** analysis is in good agreement with the **PXRD** analysis.

3.4. Thermal stability studies

The impact of the chitosan coating process on the thermal stability of **ZHN–SDS** and **ZHN–SDS–IC** were assessed using **TGA/DTG**. The difference in the weight loss of the samples was observed as a function of temperature in the range of 35–100 °C. The **TGA/DTG** curves that were obtained from the thermal stability studies of chitosan, **ZHN–SDS–Chi** and **ZHN–SDS–IC–Chi** are shown in Fig. 7.

Based on the **TGA/DTG** curves, all samples experienced multiple stages of thermal decomposition in the temperature range studied. The chitosan experienced three stages of weight loss (Fig. 7(a)), whereas the **ZHN–SDS–Chi** (Fig. 7(b)) and the **ZHN–SDS–IC–Chi** (Fig. 7(c)) experienced thermal decomposition in three and four stages of weight loss, respectively. These data were then summarised and compared with the data from the thermal stability study of the uncoated samples of **ZHN–SDS** and **ZHN–SDS–IC** that were reported in the authors' previous paper (Table 2).[31]

During the thermal decomposition of chitosan, the first weight loss occurred at 72.0 °C, with 17.8% of weight loss; the second weight loss happened at 320.3 °C, with an abrupt weight loss of 52.1%; and the third weight loss took place at 554.4 °C, with 30.2% of weight loss. A significant change in the thermal behaviour of the **ZHN–SDS** was observed after it was coated with chitosan. Before the **ZHN–SDS** chitosan coating process, the thermal decomposition occurred in two stages. The first stage happened at 107.1 °C with 3.2% of weight loss due to the loss of adsorbed and water molecule. The second stage occurred at 198.2 °C with 37.2% of weight loss due to the decomposition of **SDS**.[38] After the **ZHN–SDS** was coated with chitosan, the thermal decomposition occurred in three stages. Similar to the **ZHN–SDS**, the first thermal decompositions of **ZHN–SDS–Chi** were attributed to the loss of water which happened at 78.1 °C with a weight loss of 11.2%. The second thermal decomposition which occurred at 247.7 °C with a weight loss 51.3%, is due to the dehydration of the saccharide rings and the depolymerisation of the chitosan. The attainment of chitosan as coating material to enhance thermal stabilities was revealed based on the appearance of additional thermal decomposition peak in the **TGA/DTG** curve of the **ZHN–SDS–Chi** that indicates the combustion of **SDS** and the

collapsing of the layered structure happened at significantly high temperature (888.7 °C with 14.8 % of weight loss).

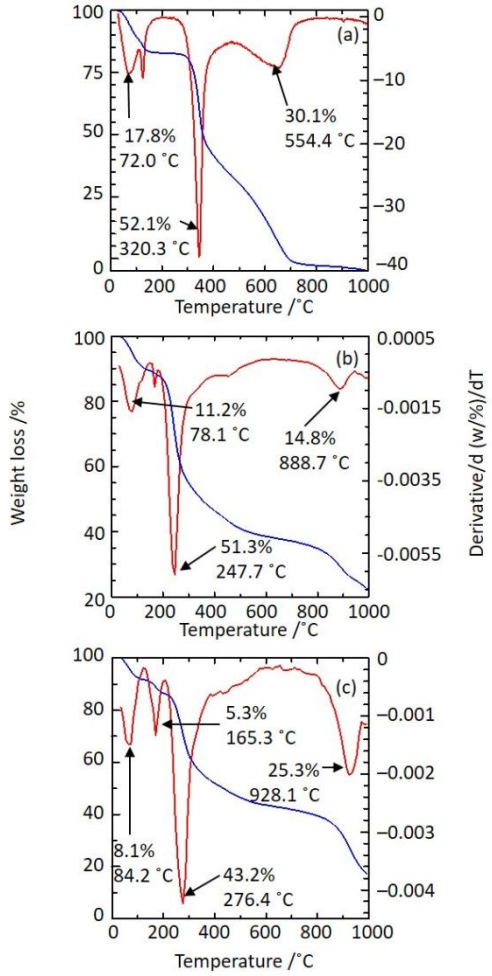

Fig. 7 TGA/DTG curves of (a) chitosan, (b) ZHN–SDS–Chi and (c) ZHN–SDS–IC–Chi nanocomposite.

The **TGA/DTG** curve for the **ZHN–SDS–IC** nanocomposite showed four stages of thermal decomposition at 108.1 °C (6.2% of weight loss), 166.4 °C (31.2% of weight loss), 264.2 °C (3.3% of weight loss) and 595.2 °C (14.3% of weight loss). The loss of sample weight at 108.1 °C was related to the elimination of adsorbed and structural water molecules, whereas the weight loss at 166.4 °C could be ascribed to the decomposition of the intercalated **IC**. The weight loss that occurred at 264.2 °C was due to the combustion of **SDS** that was present in the interlayer gallery of the **ZHN–SDS–IC**. The last weight loss occurred at 595.2 °C as the layered structure collapsed. The thermal decomposition of **ZHN–SDS–IC–Chi** also occurred in four stages at 84.0 °C (8.2% of weight loss), 165.3 °C (5.3% of weight loss), 276.2 °C (43.6% of weight loss) and 928.1 °C (25.4% of weight loss), which were attributed to similar thermal events as in the **ZHN–SDS–IC** nanocomposite. Although the temperature for the first three stages of the thermal decomposition of the **ZHN–SDS–IC** and **ZHN–SDS–IC–Chi** were not very different, it should be pointed out that a drastic change can be observed in the temperature for the fourth stage of thermal decomposition. The temperature of the fourth stage of thermal decomposition for the **ZHN–SDS–IC–Chi** (928.1 °C) was much higher than for the **ZHN–SDS–IC** (595.2 °C). This indicated a better thermal stability for the **ZHN–SDS–IC–Chi**. The major change indicated that the prominent protective effect of the chitosan on the thermal decomposition of the **ZHN–SDS–IC** was similar to **ZHN–SDS**. The potential of chitosan to enhance thermal stability of both **ZHN–SDS–Chi** and **ZHN–SDS–IC–Chi** is in good agreement with previous studies in the literature.[23,32,34]

Table 2. TGA/DTG data of weight loss for chitosan, ZHN–SDS, ZHN–SDS–Chi, ZHN–SDS–IC and ZHN–SDS–IC–Chi

Thermal decomposition		Samples				
		Chitosan	ZHN–SDS	ZHN–SDS–Chi	ZHN–SDS–IC	ZHN–SDS–IC–Chi
Stage 1	T_{max} (°C)	72.0	107.1	78.1	108.1	84.0
	Percentage (%)	17.8	3.2	11.2	6.2	8.2
Stage 2	T_{max} (°C)	320.3	198.2	247.7	166.4	165.3
	Percentage (%)	52.1	37.2	51.3	31.2	5.3
Stage 3	T_{max} (°C)	554.4	–	888.7	264.2	276.2
	Percentage (%)	30.1	–	14.8	3.3	43.6
Stage 4	T_{max} (°C)	–	–	–	595.2	928.1
	Percentage (%)	–	–	–	14.3	25.4
Ref.		Present paper	[31]	Present paper	[31]	Present paper

3.5. Surface morphology analysis

The chitosan, **ZHN–SDS**, **ZHN–SDS–Chi**, **ZHN–SDS–IC** and **ZHN–SDS–IC–Chi** nanocomposites were subjected to surface morphology analysis using FESEM, as shown in Fig. 8. The FESEM micrographs revealed a total surface morphological transformation of the **ZHN–SDS** and **ZHN–SDS–IC** after both samples underwent the chitosan coating process.

Before the **ZHN–SDS** was coated with chitosan, it had a typical morphology of a layered material, with a tabular, stacked plate–like structure and sharp edges. After it was coated with chitosan, its former plate–like structure was no longer observable. The chitosan caused the **ZHN–SDS–Chi** to have a surface morphology that resembled the surface morphology of the chitosan. As for the **ZHN–SDS–IC**, the surface morphology showed that before it was coated with the chitosan, it had a thin plate–like structure with rounded edges. The chitosan coating seemed to flatten out the surface of the **ZHN–SDS–IC–Chi**, causing the surface to be more compact and resembling the surface morphology of the pure chitosan. The results obtained from the surface morphology showed that the chitosan coating process greatly affected the surface morphology of both the **ZHN–SDS** and **ZHN–SDS–IC** nanocomposite.

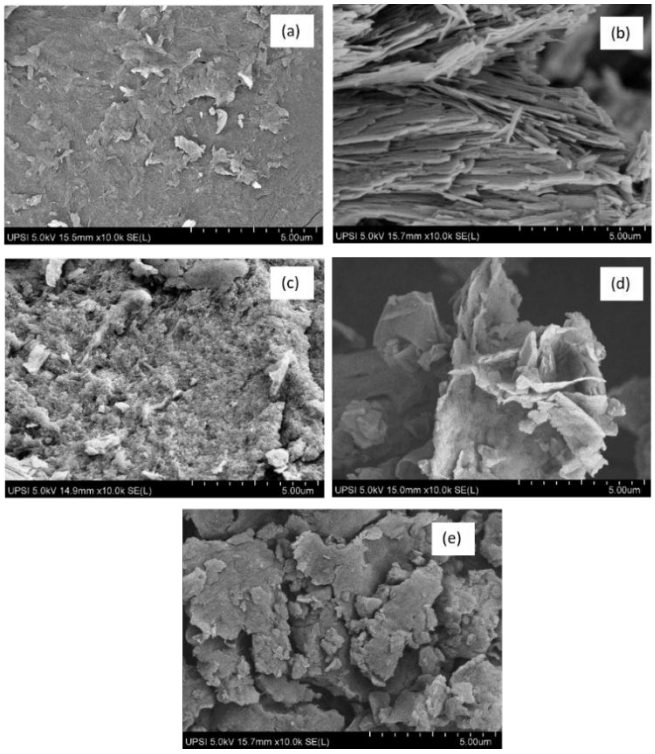

Fig. 8 Surface morphology of (a) chitosan, (b) ZHN–SDS, (c) ZHN–SDS–Chi, (d) ZHN–SDS–IC and (e) ZHN–SDS–IC–Chi.

3.6. Release Study of ZHN–SDS–IC–Chi into Single, Binary and Ternary System of Aqueous Solutions

The release behaviour of intercalated ion was influenced by the size of the nanocomposite, the properties of the reactants and the nature of interactions.[39] Here, the impact of the chitosan coating on the release behaviour of the **IC** was investigated by performing the release study of the **ZHN–SDS–IC–Chi** nanocomposite using various concentrations of Na_3PO_4, Na_2SO_4 and NaCl as the release media. The release profile for the **IC** from the **ZHN–SDS–IC–Chi** are shown in Fig. 9. The comparison with the percentage release of **IC** from **ZHN–SDS–IC** (based on the authors' previous paper) and **ZHN–SDS–IC–Chi** into single, binary and ternary system of aqueous solutions were also compared, so that the effect of the chitosan coating on the release of **IC** in release medium containing multiple type of anion can be observed (Table 3).

As shown in Fig. 9, the release behaviour of the **IC** from the interlayer gallery of **ZHN–SDS–IC–Chi** nanocomposite was strongly dependent on the nature of the release media. The release in Na_3PO_4, exhibited the highest level of cumulative release, with 96%, followed by Na_2SO_4 and NaCl, with 87% and 86%, respectively. A higher affinity for the trivalent PO_4^{3-} anions present in the Na_3PO_4 increased the tendency of the PO_4^{3-} to be attracted to the positively charged **ZHN**, and this eased the ion exchange process between the PO_4^{3-} and the **IC**. A similar trend for the release as for the **ZHN–SDS–IC** was observed when the concentration of the release media varied. This indicated that the release of the **IC** from the interlayer gallery of **ZHN–SDS–IC–Chi** was also concentration–dependent. The percentage of release was greater in a higher concentration of the release media, and it decreased when the release was performed in a lower concentration of the release media. In the release study that was performed in the aqueous solution of Na_3PO_4, the cumulative percentages released when using 0.5 M, 0.3 M and 0.1 M were 96 %, 72 % and 71%, respectively. The cumulative percentages released in aqueous Na_2SO_4 were 87%, 64% and 61%. When the release was performed in aqueous NaCl, the cumulative percentages released were 86.2%, 60.8% and 53.1%, respectively. This is because as more anions were supplied in the release media at a higher concentration, it was easier for the ion exchange to occur.[40]

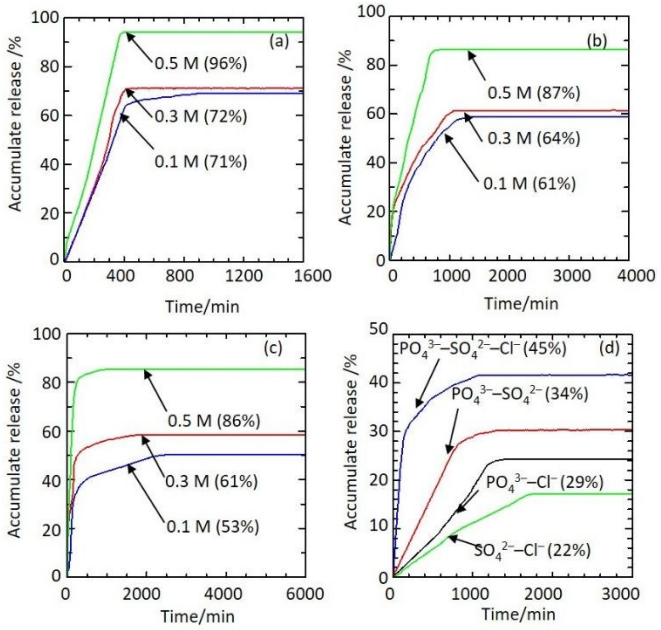

Fig. 9 Release profiles of IC from ZHN–SDS–IC-Chi nanocomposite into (a) sodium phosphate, (b) sodium sulphate and (c) sodium chloride solution in various concentrations.

Table 3. Comparison of the Release Time of **IC** from **ZHN–SDS–IC** and **ZHN–SDS–IC–Chi** into Single, Binary and Ternary Aqueous Systems of Phosphate, Sulphate and Chloride

Aqueous solutions			ZHN–SDS–IC		ZHN–SDS–IC–Chi	
			Percentage release (%)	Release time (hour)	Percentage release (%)	Release time (hour)
Single	PO_4^{3-}	0.1 M	29	5.2	71	14.7
		0.3 M	74	2.9	72	6.7
		0.5 M	91	1.4	96	6.5
	SO_4^{2-}	0.1 M	16	11.5	61	21.6
		0.3 M	83	7.9	64	17.2
		0.5 M	86	5.0	87	13.0
	Cl^-	0.1 M	6	24.6	53	41.1
		0.3 M	84	13.2	61	28.9
		0.5 M	85	9.2	86	16.7
Binary	PO_4^{3-} – SO_4^{2-}		83	22.0	34	21.8
	PO_4^{3-} – Cl^-		25	23.0	29	23.6
	SO_4^{2-} – Cl^-		22	23.8	22	28.8
Ternary	PO_4^{3-} – SO_4^{2-} – Cl^-		84	11.9	45	18.1

Ref. [31] Present paper

The release process that was performed in the aqueous solution containing Cl^- took the longest time to reach its maximum release, and the order was $Cl^- > SO_4^{2-} > PO_4^{3-}$. This could be predominantly attributed to the low charge density of the Cl^- anions, which made it less attracted to the **ZHN** layer compared to the other anions and slowed the release process.[40–42] The time taken for **IC** to be released from the interlayer gallery of **ZHN–SDS–IC–Chi** was also concentration–dependent. The release in the 0.5 M, 0.3 M and 0.1 M of aqueous NaCl required release times of 41.1 hours, 28.9 hours, 16.7 hours, respectively. As for the release in 0.5 M, 0.3 M and 0.1 M of aqueous Na_2SO_4, the release times needed were 21.6 hours, 17.2 hours and 13.0 hours, respectively. Whereas for the 0.5 M, 0.3 M and 0.1 M of aqueous NaCl, the times needed for the release were 14.7 hours, 6.7 hours and 6.5 hours, respectively. Even though the release pattern for the **ZHN–SDS–IC–Chi** and **ZHN–SDS–IC** were quite similar, the release time for the **ZHN–SDS–IC–Chi** was significantly longer compared to the **ZHN–SDS–IC** nanocomposite. The significant increase on the release time for the **IC** after the **ZHN–SDS–IC** was coated with chitosan demonstrates the potential of a chitosan coating in sustaining the release of **IC**.

In the release study of **IC** from the **ZHN–SDS–IC–Chi** nanocomposite into the binary and ternary systems of aqueous solutions, the highest percentage of accumulated release of **IC** was observed in the aqueous solution containing PO_4^{3-}–SO_4^{2-}–Cl^-, followed by PO_4^{3-}–SO_4^{2-}, PO_4^{3-}–Cl^- and SO_4^{2-}–Cl^-, with percentages of 45%, 34%, 29% and 22%, respectively. In terms of their percentage release, the presence of chitosan somehow lead to a reduction in terms of their percentage release. This trend was also similar to those reported in several previous studies that used polysaccharides as the coating material.[34,43–45] It is also noticeable that the time needed to release **IC** into the binary and ternary systems of aqueous solutions were found to be significantly extended after undergoing the chitosan coating process, regardless of their anion combination. The release process of **IC** in the ternary system of PO_4^{3-}–SO_4^{2-}–Cl^- demonstrates the shortest release time (18.1 hours) amongst all release media containing multiple types of anions, hence indicating that the release process in this mixture has the fastest release. As for the release in the aqueous solutions of PO_4^{3-}–SO_4^{2-} and PO_4^{3-}–Cl^-, the times required to achieve the maximum percentage of accumulated release of **IC** are 21.8 hours and 23.6 hours, respectively. The slowest release was obtained when the release process was performed in the aqueous solution containing SO_4^{2-}–Cl^- with a release time of 28.8 hours. These changes show that the presence of chitosan does lead to the gradual release of **IC** in multiple anion, hence proving the potential of chitosan in improving the controlled release behaviour of the **ZHN–SDS–IC** nanocomposite.

Coincident with the result obtained in this study, previous studies also pointed out the potential of chitosan in slowing the release rate of intercalated ions from their host.[22,39,46] The polycationic nature of the chitosan play a significant part in decelerating the release rate of **ZHN–SDS–IC–Chi**. The positively charged amino group on the backbone of the chitosan are capable of forming electrostatic interactions with the anionic SDS surfactant, and hence strengthen the electrostatic attractions that formerly existed between the **SDS** and the **ZHN** layers. Owing to the fact that the neutral charge **IC** exist in the hydrophobic region created by the **SDS** as micelles, the stronger electrostatic attractions formed result in the **SDS and IC** being held more tightly in the interlayer gallery of the **ZHN–SDS–IC–Chi** nanocomposite, thus increasing the time taken for the ion exchange process to occur between the anionic **SDS** surfactant and **IC**, with the incoming anions in the release media. The impact of polycationic properties of chitosan in slowing the release of intercalated guest ion is in good agreement with previous studies.[24,26,34,47–50]

Due to the hydrophilic nature of chitosan, the release of the intercalated **IC** from the hydrophilic matrices of chitosan is influenced by the rate of the matrix hydration and the gelation ability of the chitosan matrix.[51] The gelation ability of the chitosan is also due to the hygroscopic nature of it, which permit the chitosan to have a greater ability to form hydrogen bonds with water.[52] These properties considerably affect the ion diffusion, gel formation and erosion of the chitosan matrix.[53] Other than slowing the release rate of intercalated ion from its host, the gelation ability of the chitosan also assisted in reducing the burst release phenomenon for the release behaviour of the **IC** from the **ZHN–SDS–IC–Chi**. A significant reduction in the burst release was most obvious when the Na_3PO_4 was used as the release media. As can be seen from the release profile, no abrupt release was observed during the initial part of the release, which indicated that the release process occurred in sustain manner from the very beginning of it. Fast hydration allowed the formation of a gel layer and prevented the excessive release of the intercalated ions that were caused by the burst release during the early part of the release process.[53] Based on the release profile, it can be deduced that the chitosan coating immediately swelled when the nanocomposite was immersed in the release media, followed by subsequent gel layer formation and a gradual release of the **IC**. Hence, the results from the release study proved that the **ZHN–SDS–IC–Chi** is suitable for controlling the release of **IC** and the chitosan coating formulation was beneficial in increasing the **CRF** properties of the **ZHN–SDS–IC** nanocomposite.

3.7. Kinetic study of IC from the ZHN–SDS–IC–Chi nanocomposite into various aqueous solution

To obtain a deeper understanding on the release mechanism of the **IC** from the interlayer gallery of the **ZHN–SDS–IC–Chi** nanocomposite, the data collected in the release studies were fitted into several kinetic models that were zero order, first order, pseudo second order, parabolic diffusion and Fickian diffusion kinetic models. The fitting of the release data on the kinetic models are shown in Fig. 10, Fig. 11 and Fig. 12. The correlation coefficient (r^2), rate constant (k) and half time ($t_{1/2}$) were obtained from the fitting and are summarised in Table 4.

As can be seen from in Fig. 10, Fig. 11 and Fig. 12, the plot of time against t/M_i shows the best fit for the release data. This indicates the release of **IC** from the interlayer gallery of **ZHN–SDS–IC–Chi** in all release media is in good agreement with the pseudo second order kinetic model. The summarised release data in Table 4 shows that the r^2 values obtained are the highest (closest to 1) when the data were fitted into the pseudo second order kinetic model. The r^2 values obtained for the release study in the aqueous solutions of Na_3PO_4, Na_2SO_4 and NaCl are $r^2 > 0.969$, $r^2 > 870$ and $r^2 > 0.997$, respectively. The linearization of the release data into other kinetic models (zero order, first order, parabolic diffusion and Fickian diffusion) was unsatisfactory because the release data were poorly fit and resulted in low r^2 values.

View Article Online
DOI: 10.1039/D0NJ01315C

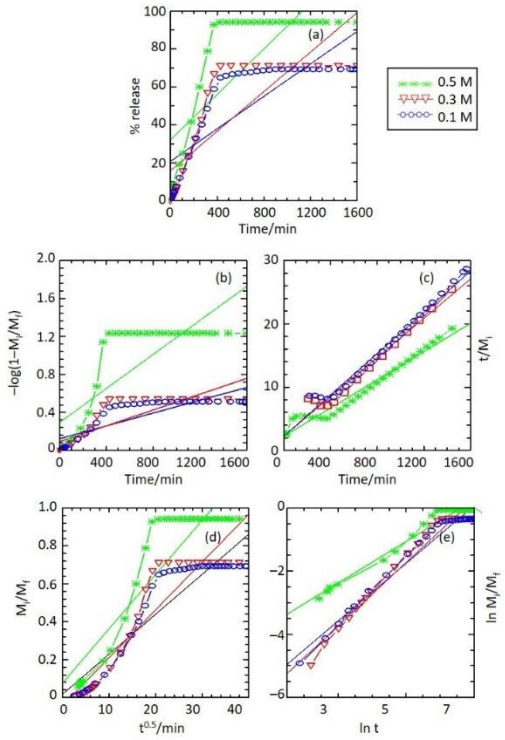

Fig. 10 Fitting of the data for IC release from ZHN–SDS–IC–Chi nanocomposite into sodium phosphate solution for the (a) zero order, (b) first order, (c) pseudo second order, (d) parabolic diffusion and (e) Fickian diffusion models.

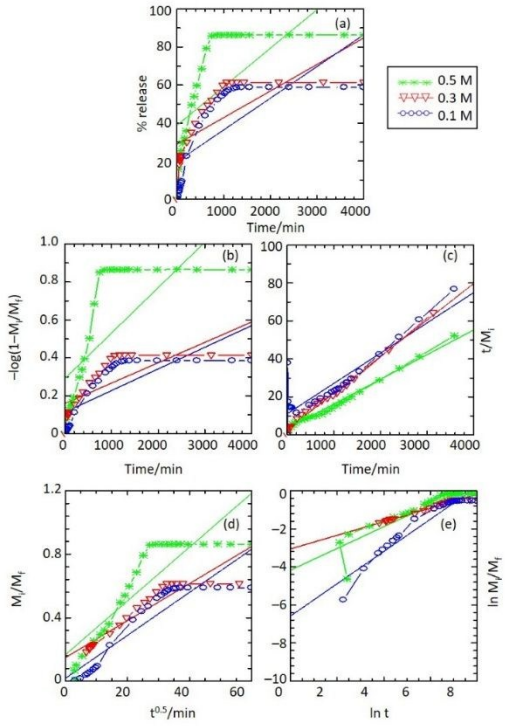

Fig. 11 Fitting of the data for IC release from ZHN–SDS–IC–Chi nanocomposite into sodium sulphate solution for the (a) zero order, (b) first order, (c) pseudo second order, (d) parabolic diffusion and (e) Fickian diffusion models.

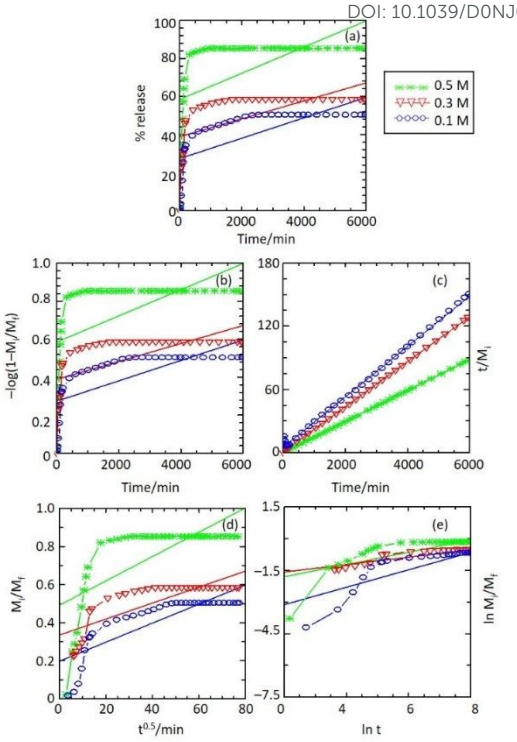

Fig. 12 Fitting of the data for IC release from ZHN–SDS–IC–Chi nanocomposite into sodium chloride solution for the (a) zero order, (b) first order, (c) pseudo second order, (d) parabolic diffusion and (e) Fickian diffusion models.

Table 4. Comparison of rate constants, *k*, and regression values, r^2, obtained from the fitting of the data of release from ZHN–SDS–IC–Chi into aqueous solution of Na_3PO_4, Na_2SO_4 and NaCl

Aqueous solution		Zero order	First order	Parabolic diffusion	Fickian diffusion	Pseudo second order		
		r^2	r^2	r^2	r^2	r^2	k (×10^{-3} s^{-1})	$t_{1/2}$
Na_3PO_4	0.1 M	0.670	0.716	0.850	0.970	0.983	0.052	243.5
	0.3 M	0.687	0.720	0.868	0.966	0.969	0.055	227.9
	0.5 M	0.633	0.678	0.972	0.826	0.972	0.062	204.5
Na_2SO_4	0.1 M	0.556	0.591	0.841	0.864	0.870	0.041	304.4
	0.3 M	0.539	0.584	0.874	0.987	0.993	0.054	234.2
	0.5 M	0.479	0.544	0.882	0.779	0.957	0.050	249.8
NaCl	0.1 M	0.491	0.551	0.683	0.710	0.997	0.098	128.8
	0.3 M	0.414	0.461	0.643	0.834	1.000	0.113	111.2
	0.5 M	0.319	0.389	0.505	0.582	0.999	0.143	87.8

The release behaviour of **IC** from the interlayer gallery of **ZHN–SDS–IC–Chi** can also be interpreted in terms of the $t_{1/2}$ values, which represent the time needed to reach half of the maximum accumulated release of the intercalated **IC**. The changes of the $t_{1/2}$ values in all release media seemed to share a similar trend, where the $t_{1/2}$ values in all release media decreased as the concentration of the release media increased. This is because the release media with

a higher concentration provided more ions, and hence more ions were available for the release process.[40] The higher concentration accelerated the release process and consequentially lowered the $t_{1/2}$ values for the release process.

The release behaviour for the **IC** that was governed by the pseudo second order kinetic model indicated that the release process started through dissolution and was subsequently followed by an ion exchange process.[54] The hygroscopic nature and gelation properties of the chitosan enabled the chitosan to form a gel layer that protected the outer surface of the **ZHN–SDS–IC** nanocomposite and sustained the release of **IC** from the nanocomposite.[45,52] The interaction between the chitosan gel layer and the water molecule in the release media hydrated the chitosan gel layer and caused the gel layer to swell. As more water penetrated into the gel layer, the swelling increased and triggered the slow dissolution of the gel layer and the **ZHN–SDS–IC** nanocomposite. This allowed the slow release of the intercalated **IC** into the release media. A further dissolution process deteriorated the chitosan gel layer and the **ZHN–SDS–IC** nanocomposite and initiated the occurrence of the release process via ion exchange.

Based on the release study, it can be concluded that the release mechanism for the **ZHN–SDS–IC** and **ZHN–SDS–IC–Chi** nanocomposites were quite similar. Both cases were governed by the pseudo second order model that indicated the release process occurred via dissolution and ion exchange. However, a significant improvement in the **CRF** properties of the **ZHN–SDS–IC** nanocomposite were observed after it was coated with chitosan. The coating process generated the formation of a chitosan gel layer that contributed to slowing the release process and increasing the $t_{1/2}$ values.

Conclusion

Even though there are numerous previous studies that reported on the **CRF** of pesticides, most of the pesticides use in the system exist in anionic nature. The neutral charge guest ion may not be directly intercalated into the interlayer gallery of layered metal hydroxides owing to the neutral charge possessed by this ion. As a result of their challenging intercalation process, fewer studies have reported on the **CRF** of neutral charge pesticides, as compared to the anionic pesticides. The results reported in this work demonstrate the success of the chitosan coating on the **ZHN–SDS–IC** nanocomposite in a simple, easy and less time–consuming process, as an endeavour for enhancing the **CRF** of neutral charge pesticides. The characterisation study performed using **PXRD** and **FTIR** revealed that the chitosan process did not interfere with the types of ions intercalated in the **ZHN–SDS–IC** nanocomposite. A slight increase in the interlayer gallery height allowed the **ZHN–SDS–IC–Chi** nanocomposite to preserve its vertical monolayer arrangement. The chitosan coating process was proven to increase the thermal stability of **ZHN–SDS–IC–Chi** nanocomposite and transform their surface morphology into a flatter and more compact plate–like structure. The results from the release study provided insight on the suitability of chitosan to be used as coating material and its potential to prolong the release of the intercalated **IC** from the **ZHN–SDS–IC** nanocomposite. The highest percentage of the cumulative release was observed when the **ZHN–SDS–IC–Chi** nanocomposite was immersed in the aqueous solutions of Na_3PO_4, in the order of Na_3PO_4 > Na_2SO_4 > NaCl. The slowest release process was observed when the NaCl was used as the release media, and the release process was also found to be concentration–dependent. The enhancement in the release behaviour of the **ZHN–SDS–IC–Chi** nanocomposite was due to the hydrophilic and hygroscopic nature of chitosan, which made it possible for the chitosan to form a gel layer in the hydrated environment. The kinetic study showed that the release of **IC** from the **ZHN–SDS–IC–Chi** was governed by the pseudo second order model and indicated that the release mechanism was via dissolution and the ion exchange process. It is always worthwhile to give an extra effort to develop a new pesticide that satisfies both economic and ecological demand. Thus, the potential of chitosan to enhance the controlled release properties of the **ZHN–SDS–IC–Chi** can hopefully help to reduce the risk of pollution due to the excessive use of pesticide in the agricultural sector.

Conflict of interest

None declared.

Acknowledgement

The author wishes to thank UPSI and Ministry of Education Malaysia for the support during completing the research. This work was supported by the GPU-RISING STAR Grant No. 2019−0119−103−01.

Notes and references

1 S. Kumaran, A. Kamari, M. M. Abdulrasool, S. T. S. Wong, J. Jumadi, S. N. M. Yusoff and S. Ishak, *J. Phys. Conf. Ser.*, , DOI:10.1088/1742-6596/1397/1/012030.

2 S. N. M. Yusoff, A. Kamari, S. Ishak, J. Jumadi, M. M. Abdulrasool, S. Kumaran and S. T. S. Wong, *J. Phys. Conf. Ser.*, , DOI:10.1088/1742-6596/1397/1/012026.

3 I. N. F. A. Aziz, S. H. Sarijo, F. S. M. R. Y. Rajidi and M. Musa, *J. Porous Mater.*, 2019, **26**, 717–722.

4 M. Z. Hussein, N. F. Nazarudin, S. H. Sarijo and M. A. Yarmo, *J. Nanomater.*, 2012, **2012**, 1–10.

5 G. Gwak, S. Paek and J. Oh, 2012, 5269–5275.

6 A. Matalanis, O. G. Jones and D. J. McClements, *Food Hydrocoll.*, 2011, **25**, 1865–1880.

7 Q. Z. Yang, Y. Y. Chang and H. Z. Zhao, *Water Res.*, 2013, **47**, 6712–6718.

8 J. Liu, X. Zhang and Y. Zhang, *ACS Appl. Mater. Interfaces*, 2015, **7**, 11180–11188.

9 R. Otero, J. M. Fernández, M. A. Ulibarri, R. Celis and F. Bruna, *Appl. Clay Sci.*, 2012, **65–66**, 72–79.

10 L. M. Varca, *Agric. Water Manag.*, 2012, **106**, 35–41.

11 G. Preetha, J. Stanley, S. Suresh and R. Samiyappan, *Chemosphere*, 2010, **80**, 498–503.

12 M. Z. Bin Hussein, A. H. Yahaya, Z. Zainal and L. H. Kian, *Sci. Technol. Adv. Mater.*, 2005, **6**, 956–962.

13 S. Dubey, V. Jhelum and P. K. Patanjali, *J. Sci. Ind. Res. (India).*, 2011, **70**, 105–112.

14 A. M. Bashi, M. Z. Hussein, Z. Zainal and D. Tichit, *J. Solid State Chem.*, 2013, **203**, 19–24.

15 M. Z. Hussein, N. S. S. A. Rahman, S. H. Sarijo and Z. Zainal, *Int. J. Mol. Sci.*, 2012, **13**, 7328–7342.

16 M. Z. Hussein, N. Hashim, A. H. Yahaya and Z. Zainal, *Solid State Sci.*, 2010, **12**, 770–775.

17 S. M. N. Mohsin, M. Z. Hussein, S. H. Sarijo, S. Fakurazi, P.

Arulselvan and T.-Y. Y. Hin, *Chem. Cent. J.*, 2013, **7**, 26.
18 N. Hashim, Z. Muda, S. A. Hamid, I. Isa, A. Kamari, A. Mohamed, Z. Hussein and S. A. Ghani, *J. Phys. Chem. Sci.*, 2014, **1**, 1–6.
19 M. Z. bin Hussein, M. Y. Ghotbi, A. H. Yahaya and M. Z. Abd Rahman, *Mater. Chem. Phys.*, 2009, **113**, 491–496.
20 B. Saifullah, M. Z. Hussein, S. H. Hussein-Al-Ali, P. Arulselvan and S. Fakurazi, *Chem. Cent. J.*, 2013, **7**, 72.
21 E. Corradini, M. R. De Moura and L. H. C. Mattoso, *Express Polym. Lett.*, 2010, **4**, 509–515.
22 Y. Luo, Z. Teng, Y. Li and Q. Wang, *Carbohydr. Polym.*, 2015, **122**, 221–229.
23 S. A. Agnihotri and T. M. Aminabhavi, *J. Control. Release*, 2004, **96**, 245–259.
24 I. Alemzadeh and M. Vossoughi, *Chem. Eng. Process.*, 2011, **41**, 707–710.
25 K. Nakagawa, N. Sowasod, W. Tanthapanichakoon and T. Charinpanitkul, *LWT - Food Sci. Technol.*, 2013, **54**, 600–605.
26 S. Woranuch and R. Yoksan, *Carbohydr. Polym.*, 2013, **96**, 578–585.
27 I. Ishaaya and A. R. Horowitz, in *Insecticides with novel modes of action*, eds. I. Ishaaya and D. Degheele, Springer, Berlin, Heidelberg, 1998, pp. 1–24.
28 S. Hervé Thany, *Insect Nicotinic Acetylcholine Receptors*, 2010.
29 I. Yamamoto and J. E. Casida, *Nicotinoid Insecticides and the Nicotinic Acetylcholine Receptor*, 1999.
30 S. Jorgen, *Chemical Pesticides Mode of Action and Toxicology*, CRC Press, Boca Raton, 2004.
31 S. N. M. Sharif, N. Hashim, I. M. Isa, S. A. Bakar, M. I. Saidin, M. S. Ahmad, M. Mamat and M. Z. Hussein, *J. Porous Mater.*, 2020, **27**, 473–486.
32 Y. Luo, T. T. Y. Wang, Z. Teng, P. Chen, J. Sun and Q. Wang, *Food Chem.*, 2013, **139**, 224–230.
33 Z. Teng, Y. Luo and Q. Wang, *J. Agric. Food Chem.*, 2012, **60**, 2712–2720.
34 S. F. Hosseini, M. Zandi, M. Rezaei and F. Farahmandghavi, *Carbohydr. Polym.*, 2013, **95**, 50–56.
35 D. P. Qiu, W. G. Hou, J. Xu, J. Liu and S. Liu, *Chinese J. Chem.*, 2009, **27**, 1879–1885.
36 M. Li, S. Chen, F. Ni, Y. Wang and L. Wang, *Electrochim. Acta*, 2008, **53**, 7255–7260.
37 Q. Tao, J. Yuan, R. L. Frost, H. He, P. Yuan and J. Zhu, *Appl. Clay Sci.*, 2009, **45**, 262–269.
38 N. Hashim, S. N. M. Sharif, Z. Muda, I. M. Isa, N. M. Ali, S. A. Bakar, S. M. Sidik and M. Z. Hussein, *Mater. Res. Innov.*, 2018, **23**, 233–245.
39 R. Grillo, A. E. S. Pereira, C. S. Nishisaka, R. De Lima, K. Oehlke, R. Greiner and L. F. Fraceto, *J. Hazard. Mater.*, 2014, **278**, 163–171.
40 S. Li, Y. Shen, M. Xiao, D. Liu and L. Fan, *Arab. J. Chem.*, 2015, **12**, 2563–2571.
41 S. A. I. S. M. Ghazali, M. Z. Hussein and S. H. Sarijo, *Nanoscale Res. Lett.*, 2013, **8**, 1–8.
42 S. H. Sarijo, S. A. I. S. M. Ghazali, M. Z. Hussein and A. H. Ahmad, *Mater. Today Proc.*, 2015, **2**, 345–354.
43 Z. Rezvani and M. Shahbaei, *Polym. Compos.*, 2014, **36**, 1819–1825.
44 L. N. M. Ribeiro, A. C. S. Alcântara, M. Darder, P. Aranda, F. M. Araújo-Moreira and E. Ruiz-Hitzky, *Int. J. Pharm.*, 2014, **463**, 1–9.
45 N. B. Allou, A. Yadav, M. Pal and R. L. Goswamee, *Carbohydr. Polym.*, 2018, **186**, 282–289.
46 B. P. Koppolu, S. G. Smith, S. Ravindranathan, S. Jayanthi, T. K. Suresh Kumar and D. A. Zaharoff, *Biomaterials*, 2014, **35**, 4382–4389.
47 C. Sanjai, S. Kothan, P. Gonil, S. Saesoo and W. Sajomsang, *Carbohydr. Polym.*, 2014, **104**, 231–237.
48 J. D. Bumgardner, A. Des Rieux, N. Duhem, J. Dutta, P. K. Dutta, T. Furuike, C. Gao, W. O. Haggard, R. Jayakumar, J. A. Jennings, C. Jerome, M. R. Leedy, X. Liu, L.Ma, Z. Mao, H. J. Martin, R. A. A. Muzzarell, P. A. Norowski, N. Nwe, M. Prabaharan, V. Preat, H. Ragelle, K. Rinki, R. Riva and H. Tamura, *Advances in Polymer Science*, Springer-Verlag Berlin Heidelberg, London, 2011.
49 D. Davidson and F. X. Gu, *J. Agric. Food Chem.*, 2012, **60**, 870–876.
50 M. Vemmer and A. V. Patel, *Biol. Control*, 2013, **67**, 380–389.
51 J. Nunthanid, M. Laungtana-Anan, P. Sriamornsak, S. Limmatvapirat, S. Puttipipatkhachorn, L. Y. Lim and E. Khor, *J. Control. Release*, 2004, **99**, 15–26.
52 E. Szymańska and K. Winnicka, *Mar. Drugs*, 2015, **13**, 1819–1846.
53 R. M. Lucinda-Silva, H. R. N. Salgado and R. C. Evangelista, *Carbohydr. Polym.*, 2010, **81**, 260–268.
54 N. Hashim, Z. Muda, S. A. Hamid, I. M. Isa, A. Kamari, A. Mohamed, M. Z. Hussein and S. A. Ghani, *J. Phys. Chem. Sci.*, 2014, **1**, 1–6.

View Article Online
DOI: 10.1039/D0NJ01315C

Graphical abstract